Dimensioning of automated regenerative cooling: Setting of high-end experiment

L Taddeo, Nicolas Gascoin, I Fedioun, K Chetehouna, L Lamoot, G Fau

Dimensioning of Automated Regenerative Cooling: Setting of High-End Experiment

L. Taddeo[11], N. Gascoin[1], I. Fedioun[2], K. Chetehouna[1], L. Lamoot[1], G. Fau[1]

[1]INSA Centre Val de Loire, PRISME, 88 boulevard Lahitolle, 18000 Bourges, France

[2]CNRS ICARE, Avenue de la recherche, 45100 Orléans, France

Highlights

- A unique remote-controlled experimental bench is integrated for regeneratively hydrocarbon cooled combustor
- A nozzle-like device trapping pyrolysis-formed carbon was designed to depressurize fuel before injection.
- Similitude rules were used to reproduce real operating conditions (Pyrolysis rate, Surface/Volume heat flux…)
- The possibility to operate over large testing conditions (fuel flow rate from 70 to 100 mg/s, pressure up to 50 bar, max fuel temperature 1500 K, Equivalence ratio from 0.8 to 1.1)
- The possibility to get complete fuel pyrolysis at lab scale was demonstrated, similarly to realistic operating scale

Abstract

Regenerative cooling is a hot topic as it contributes to energy saving and energy conversion, for

[1] Corresponding Authors : Ing. Lucio TADDEO, lucio.taddeo@insa-cvl.fr; Pr Dr Ing Nicolas GASCOIN, nicolas.gascoin@insa-cvl.fr

example within high speed propulsion or chemical plants frameworks. Considering the use of this technology in fuel-cooled hypersonic structures, the propellant duality in terms of functions (coolant and fuel) makes the thermal and combustion management to be quite challenging. Dynamics of the system must be studied in order to develop regulation and control strategies which should be performed with a response time lower than the lowest characteristic time found in supersonic combustion ramjet, i.e. about 1 ms. The present work aims at setting experiments at lab scale by simplifying the additional difficulty of supersonic flow. A combustion chamber is dimensioned with similitude rules in terms of heat flux density, conversion rate, chemical compositions, dynamics. Computational Fluid Dynamics and analytical calculations are developed to dimension the experimental bench. Instead of using trial-error approach when setting up an experiment, this prediction work ensures having appropriate regulation dynamics for latter model and control developments. It has been found that a pyrolysis rate up to 100% can be obtained using ethylene as fuel at 50 bar and 1200 K and with a residence time of about 100 s. Combustion with air (adiabatic flame temperature up to 2400 K) will provide the required heat flux density. The operating range in terms of fuel pressure (10-50 bar), of fuel mass flow rates (50-100 mg s^{-1}) and of equivalence ratio (0.8 to 1.0) have been certified.

Nomenclature

$C_{1\varepsilon}$	numerical constant (1.44)
$C_{2\varepsilon}$	numerical constant (1.92)
C_{μ}	numerical constant (0.09)
c_p	heat capacity
D	diameter
ΔP	pressure drops
$\Delta H_{dec\ fuel}$	enthalpy of decomposition

ER	fuel to oxidizer molar ratio
E	energy
F	view factor (1)
g	gravitational acceleration
G_k	generation of turbulence kinetic energy due to the mean velocity gradients
G_b	generation of turbulence kinetic energy due to buoyancy
H	height
h	convective heat transfer coefficient
$\vec{J}_j$	diffusion flux of species j
k	turbulence kinetic energy
k_{eff}	effective thermal conductivity
K_D	Darcy's permeability
k_{ther}	thermal conductivity
l	cooling channel length
L_d	porous disks thickness
$\dot{m}$	mass flow rate
Q	volumetric flow rate
S_d	porous disks cross section
S_w	combustion chamber wall surface
t	time
T	temperature
$u_{i,j,k}$	velocity components
$x_{i,j,k}$	cartesian coordinates
Y_M	dissipation due to turbulence

Greek Symbols

ε	turbulence rate of dissipation

ε_e	burned gases emissivity
Φ	heat flux density
μ	dynamic viscosity
μ_t	turbulent dynamic viscosity
ρ	density
$\bar{\bar{\tau}}_{eff}$	effective stress tensor

Subscripts

burned gases	combustion products
combustor	combustion chamber
cool channel	cooling channel
exit	combustion chamber exit
external	cooling channel side
fuel	fuel (n-dodecane/ethylene)
in	cooling channel entrance
internal	combustion chamber side
out	cooling channel exit
oxid	oxidizer (air)
wall	combustion chamber wall

1. Introduction

Hypersonic flight (over Mach 5) is a very attractive technology, especially in terms of flight time reduction (e.g. Bruxelles-Sydney in two hours). Its most peculiar features, i.e. high velocity and long-distance utilization, can also fit to other technological applications, like air launched strike weapons, space transport vehicles, ground launched satellite [1-4].

Hydrogen and hydrocarbons propelled hypersonic flights are expected to be achieved in the coming years by means of Supersonic Combustion Ramjet (SCRamjet) engines [5]. This kind of air-breathing engines uses the vehicle forward motion to compress incoming air, without

any rotary compressor.

SCRamjet suffers from two main problems:

1. High temperature values in combustion chamber. Maximum total temperature can achieve values as high as 4500 K [5]. That determines a dramatic heat load toward the inner wall of the engine (up to 25 MW m^{-2}) [4,6,7], that even composite materials cannot withstand;
2. Low time allocated for the combustion. Reactants (fuel-oxidizer) residence time in the combustion chamber is of about 1 ms [8]. Because of the high values of ignition delay times for liquid hydrocarbons, that raises difficulties for the combustion process to be regularly carried out [5,7].

Regenerative cooling is one of the most widely applied cooling techniques in liquid propellant rocket engines [9,10]. Many studies, particularly numerical, have already been performed on it. It has proven to be a suitable and effective solution for both problems 1) and 2) for hydrocarbon-fuelled vehicles [11,12]. Fuel acts as a coolant, flowing through cooling channels located between the inner and the outer wall of the engine, before being injected into the combustion chamber. A counter-flow heat exchange between a liquid or supercritical domain (fuel) and a gaseous domain (burned gases) is thus established. The possibility of exploiting regenerative cooling when non-hydrocarbon fuels are used has also undergone numerical investigations. Hydrocarbons are preferred for flight whose Mach number is under 8, whether hydrogen is preferred when aiming at achieving Mach number over 8 [3]. The cooling capacity of hydrogen is, when compared to that of kerosene, far lower, especially because of the difficulty for it to perform endothermic conversion [6]. Moreover, its relatively high cost discourages its utilization [13].

If an hydrocarbon propellant is used, fuel undergoes pyrolysis when heated above 800 K.

The endothermic behavior of the chemical reactions enhances its cooling capacity (corresponding to a chemical heat sink of about 1-1.5 MJ kg^{-1}, being 3-4 MJ kg^{-1} the sensible heat sink [14]). The complex chemistry of light and heavy hydrocarbon fuels pyrolysis has already been object of studies, especially in the petro-chemical fields [15]. Pyrolysis phenomena generate many species like hydrogen and light hydrocarbons (ethane, ethylene, acetylene, etc.). The ignition delay times of the light pyrolysis products are very low when compared to the initial heavy fuel. That allows the combustion process to get completely realized in the combustion chamber, thus improving the rocket engine performance. A major challenge associated to the dual function of the fuel (coolant and fuel) is to provide a regulation strategy which could be compatible with the dynamics of the supersonic vehicles [5]. Indeed, increasing the thrust by increasing fuel mass flow rate may conduct to a thrust decrease because in correspondence of fuel injection increase, heat load available to pyrolyse the fuel would remain constant. Only transient evolution of heat load through the structure could provide more energy to pyrolyse the increased incoming coolant fuel. This is a strongly transient, coupled and multiphasic topic. This negative loop is illustrated in Fig. 1. It can also be noticed that controlling the thrust should be done with response times lower than 1 s (which corresponds to a traveled distance of 1 km at Mach 5, quite a lot when piloting a flying vehicle).

Figure 1. should be placed here

System control and thermal management are thus a very harsh task, because of the strong coupling between pyrolysis and combustion. The impact of the most important operating parameter, i.e. fuel mass flow rate, on the engine thrust is still not clear. A further complication is the strong transient nature of these coupled phenomena in on-board application [5]. In addition, side effects like cooling channels blockage can be found, as fuel pyrolysis also originates coke deposits, that can stick to the wall of the channels [15-17]. That raises serious concerns because of two possible consequences:

1. A decrease in the cooling capacity of system;
2. The danger for the cooling channels to be jammed by coke.

In this sense, the COMPARER program developed by MBDA-France and by the University of Orleans [3,4] aimed at identifying, by means of both a numerical and an experimental analysis of the system, how the already mentioned operating parameter (fuel mass flow rate) interferes with pyrolysis-combustion coupling. A numerical code, the so-called RESPIRE code, able to simulate hypersonic vehicles regenerative cooling realized using a hydrocarbon liquid propellant, was developed and the dynamics of the coupled phenomena were determined. This program has highlighted the complexity of the matter, emphasizing the necessity of an empirical analysis of the system. The on-going activity is now focused on the implementation of a coupled experiment (fuel pyrolysis in cooling channels + fuel consumption in combustion chamber) to verify and validate the numerically acquired knowledge and particularly the dynamics of the phenomena. This step is necessary for a latter development of on-board regulation strategies (thermal management + thrust control).

The present work aims at setting up a remote controlled experimental test bench suitable for the empirical analysis of pyrolysis-combustion coupling, by considering subsonic combustion as a first step to limit the test facility requirements. To do that, pre-dimensioning of combustion chamber and cooling channels (geometry, dimensions, operating conditions) has been performed by means of numerical simulations. ANSYS FLUENT CFD software has been used. Turbulence has been modelled by using k-ε model, with wall-functions near wall treatment. Additional analytical calculations have been developed following similitude rules in order to predict the dynamics of the bench.

This quite original approach contributes to set up high-end experiments which will assure an improvement in the knowledge of the scientific and engineering community.

2. Materials and Methods

2.1. 0-D analytical calculations for dynamics characterization in case of liquid fuel

The following configuration (fig. 2) has been considered to provide a first insight into heat transfer orders of magnitude and on system dynamics. Three domains have been defined: a liquid domain (fuel), a solid domain (combustion chamber wall) and a gaseous domain (burned gases).

Figure 2. should be placed here

Heat transfer within the fuel (liquid domain) was modelled with equation 1:

$$\Phi_{fuel} = \Phi_{fuel,\ sensible} + \Phi_{fuel,\ chemical} \quad (1)$$

$$\Phi_{fuel,\ sensible} = \dot{m}_{fuel}\, c_{p,\,fuel} \left(T_{fuel,\ out} - T_{fuel,\ in}\right) \quad (2)$$

$$\Phi_{fuel,\ chemical} = \dot{m}_{fuel}\, \Delta H_{dec\ fuel} \quad (3)$$

Equation 2 and 3 represent respectively the sensible heat and the chemical heat absorbed by the fuel, the latter deriving from the endothermic behavior of pyrolysis reactions.

Heat transfer within the burned gases (gaseous domain) was modelled with equation 4:

$$\Phi_{burned\ gases} = \Phi_{burned\ gases,\ convective} + \Phi_{burned\ gases,\ radiative} + \Phi_{burned\ gases,\ loss} \quad (4)$$

$$\Phi_{burned\ gases,\ convective} = h_{burn\ gases}\, S \left(T_{burned\ gases,exit} - T_{wall,\ internal}\right) \quad (5)$$

$$\Phi_{burned\ gases,\ radiative} = \sigma\, \varepsilon_{burned\ gases}\, S\, F \left(T^4_{burned\ gases,exit} - T^4_{wall,\ internal}\right) \quad (6)$$

$$\Phi_{burned\ gases,\ loss} = 0.20\, \Phi_{burned\ gases} \quad (7)$$

Equation 5 and 6 represent respectively heat transfer from the hot gases to the combustion chamber wall by means of convection and radiation. Equation 7 permits to take into account the amount of heat lost with the flue gases.

Heat transfer within the combustion chamber wall (solid domain) was modelled with equation 8:

$$\Phi_{wall} = \Phi_{burned\ gases,\ convective} + \Phi_{burned\ gases,\ radiative} = \Phi_{fuel,\ convective} \quad (8)$$

$$\Phi_{fuel,\ convective} = h_{fuel}\, S\left(T_{wall,\ external} - T_{fuel,\ in}\right) \quad (9)$$

Equation 9 represents heat transfer by convection through the fuel.

2.2. Nozzle design for pressure decrease

Being the intention of the authors is to carry out ambient pressure combustion, a specific system for decreasing fuel pressure is required. In fact ethylene flowing into the cooling channel is expected to be at high pressure and possibly at supercritical state. A nozzle-like device has so been designed. It is made of an external casing (Fig. 3) able to sustain high pressures and high temperatures in which several stainless steel porous disks are inserted with decreasing porosity and permeability. Depending on the characteristics of the porous media, pressure drops can be estimated by the Brinkman law **Erreur ! Source du renvoi introuvable.**. The succession of porous media also enables getting coke particles and separating them as a function of their granulometry for a subsequent estimation of the coking and blocking effect which are typical of pyrolysis through porous media **Erreur ! Source du renvoi introuvable.**.

Figure 3. should be placed here

Knowing fuel mass flow rate and the porous media characteristics, pressure drops can be estimated through each porous media by Darcy's law:

$$Q = K_D\, S_d\, \frac{\Delta P}{\rho\, g\, L_d} \quad (10)$$

2.3. CFD models and assumptions

The numerical simulation of the cooling channel and of the combustion chamber has been realized by using ANSYS FLUENT CFD software. On the basis of empirical estimations made earlier on the velocity fields characterizing the system (evaluation of Reynolds numbers), whose results will be presented in section 3, turbulent conditions are expected into the combustion chamber. So, in this work, the choice has fall on the standard k-ε model (class of Reynolds Averaged Navier Stokes – RANS - turbulence models). That is justified by the fact that k-ε model is found in the established practice for this specific class of problems and because of the expected level of accuracy and the available computational resources **Erreur ! Source du renvoi introuvable.**. The equations governing the transport of the averaged flow quantities are **Erreur ! Source du renvoi introuvable.**:

$$\frac{\partial \rho}{\partial t} + \frac{\partial}{\partial x_i}(\rho u_i) = 0 \tag{11}$$

$$\frac{\partial}{\partial t}(\rho u_i) + \frac{\partial}{\partial x_j}(\rho u_i u_j) = -\frac{\partial p}{\partial x_i} + \frac{\partial}{\partial x_j}\left[\mu\left(\frac{\partial u_i}{\partial x_j} + \frac{\partial u_j}{\partial x_i} - \frac{2}{3}\delta_{ij}\frac{\partial u_k}{\partial x_k}\right)\right] + \frac{\partial}{\partial x_j}\left(-\rho\overline{u_i{}'u_j{}'}\right) \tag{12}$$

The standard k-ε model is a semi-empirical model based on the above mentioned transport equations, where:

$$-\rho\overline{u'_i u'_j} = \mu_t\left(\frac{\partial u_i}{\partial x_j} + \frac{\partial u_j}{\partial x_i}\right) - \frac{2}{3}\left(\rho k + \mu_t\frac{\partial u_k}{\partial x_k}\right)\delta_{ij} \tag{13}$$

The turbulent viscosity, μ_t, is defined as follows:

$$\mu_t = \rho C_\mu \frac{k^2}{\varepsilon} \tag{14}$$

The turbulence kinetic energy, k, and its rate of dissipation, ε, are obtained from the following transport equations:

$$\frac{\partial}{\partial t}(\rho k) + \frac{\partial}{\partial x_i}(\rho k u_i) = \frac{\partial}{\partial x_j}\left[\left(\mu + \frac{\mu_t}{\sigma_k}\right)\frac{\partial k}{\partial x_j}\right] + G_k + G_b - \rho\varepsilon - Y_M + S_k \quad (15)$$

$$\frac{\partial}{\partial t}(\rho\varepsilon) + \frac{\partial}{\partial x_i}(\rho\varepsilon u_i) = \frac{\partial}{\partial x_j}\left[\left(\mu + \frac{\mu_t}{\sigma_\varepsilon}\right)\frac{\partial \varepsilon}{\partial x_j}\right] + C_{1\varepsilon}\frac{\varepsilon}{k}(G_k + C_{3\varepsilon}G_b) - C_{2\varepsilon}\rho\frac{\varepsilon^2}{k} + S_\varepsilon \quad (16)$$

The default values of the constants present in the transport equations of k and ε have been determined from experiments with air and water in well defined turbulent conditions.

The transport of energy E is described solving equation 9:

$$\frac{\partial}{\partial t}(\rho E) + \nabla\cdot\left(\vec{v}(\rho E + p)\right) = \nabla\cdot\left(k_{eff}\nabla T + \sum_j h_j \vec{J}_j + (\bar{\bar{\tau}}_{eff}\cdot\vec{v})\right) + S_h \quad (17)$$

The first three terms on the right-hand side of the above reported equation represent respectively energy transfer due to conduction, species diffusion, and viscous dissipation. In particular:

$$E = h - \frac{p}{\rho} + \frac{v^2}{2} \quad (18)$$

2.4. Geometry and dimensions estimated by CFD analysis

Estimation of the following parameters is expected from CFD results: height and diameter of the combustor, length and diameter of the rolled-up stainless steel tube which, passing through the combustion chamber, will simulate the cooling channels of regenerative cooled ramjets, heat flux density from the burned gas to the fuel, fuel and oxidizer mass flow rates and maximum wall temperature in the combustor (to ensure its withstanding for long run operation). The basic condition to respect is to get fuel conversion at the cooling channel outlet over 50% wt. Moreover, temperatures achieved by all components should not overpass 1400 K. Temperatures of the fuel flowing into the cooling channel are also expected to be derived from CFD analysis.

The geometrical configuration adopted for the combustion chamber is shown in figure 4. It is computed considering 2-D axisymmetric assumptions.

Figure 4. should be placed here

With the help of data that can be found in literature, referring to cases characterized by similar fluid dynamics, it is possible to anticipate which are the attributes of the flow. Being the flow confined, it will probably be influenced by the walls geometry. Considering the aims of the authors, who do not wish to get into the details regarding heat/mass transfer, but just qualitatively compute the overall test bench, the near-wall region has been solved by using the wall-functions approach. For engineering purpose, this approach saves computational resources, as the viscosity affected near wall region does not need to be solved.

The reliability of wall function approach for a given turbulence model requires for y^+ values to be within a certain range. When using wall function approach, values ranging from 10 to 300 are required **Erreur ! Source du renvoi introuvable.**. The meshes used in this works are uniform grids. Fig. 5 refer to that of case $D_{combustor}$=8cm.

Figure 5. should be placed here

Their main features are reported in tab. 1.

Table 1. should be placed here

The use of the above reported meshes allows values of y^+ ranging from 5 to 40 in correspondence of the combustion chamber walls. Values under 10 are achieved along the wall of the cooling channel, where a laminar flow is expected. That does not affect the reliability of the results. Three different combustion chamber diameters have been taken into account, respectively 8 cm, 10 cm and 12 cm. Three different values of the equivalence ratio (fuel to oxidizer molar ratio), ranging from 0.8 to 1.0, have been considered, to move from a lean to a stoichiometric combustion (to match with lean combustion expected on-board on

hypersonic vehicles). Operating in lab conditions, fuel mass flow rate was maintained constant (0.1 g s^{-1}) for safety reasons. In order to vary equivalence ratio ER, air mass flow rate varies, from 1.47 g s^{-1} (stoichiometric combustion) to 1.84 g s^{-1}, as shown in table 2.

Table 2. should be placed here

The flame was simulated by means of an axisymmetric jet of air, with a diameter of 2 cm. Whatever the case, jet temperature corresponds to that it would achieve in the event of combustion in adiabatic conditions. The initial temperature of the fuel/oxidizer mixture has been set at 400 K, by considering a temperature of the fuel entering the burner after flowing into the cooling channel of 1000 K, which is supposed closer to real operating than the ambient.

Air and ethylene properties have been defined as polynomial functions of temperature. The properties both of the stainless steel tubes and of the ceramic refractories blanket, i.e. density, thermal conductivity and heat capacity, have been defined by the authors. They are considered as constants and reported in table 3.

Table 3. should be placed here

Adiabatic conditions have been considered on the external stainless steel casing (fig. 4), whose temperature has been set to 300 K. The Navier-Stokes equations are solved in axisymmetric configuration. Boundaries conditions have been imposed as follows:

1 Mass Flow Inlet at the entrance of the reacting mixture in the burner and at the entrance of the fuel in the helix-like stainless steel tube;
2 Pressure Outlet at the exit of the burned gases from the burner and of the exit of the fuel from the helix-like stainless steel tube;
3 Wall in correspondence of all the other surfaces.

They are illustrated in figure 6. Except for the highlighted ones, all the other surfaces are defined as wall.

Figure 6. should be placed here

3. Results and discussion

Combustor dimensioning consists mainly in choosing the optimum diameter. To summarize, on the basis of the above exposed considerations, the choice must be based on:

1. the maximum temperature achieved by the fuel: ethylene pyrolysis requires temperature as high as 1200K **Erreur ! Source du renvoi introuvable.**;
2. the temperature achieved by the helix-like stainless steel tube: 316L stainless steel can not be exposed to temperature over 1400 K **Erreur ! Source du renvoi introuvable.**.

The second parameter is crucial, as at too high temperatures the mechanical properties of the stainless steel dangerously decline **Erreur ! Source du renvoi introuvable.**.

As already said, turbulent flow can be expected in the combustor (Reynolds number evaluation, tab. 4). The results of the numerical simulations confirm the validity of this assumption.

Table 4. should be placed here

3.1. Temperature fields and heat flux of burned gases and fuel

Temperature distributions for the different values of combustor diameter $D_{combustor}$ and of equivalence ratio ER have been evaluated. Temperature contours are reported in fig. 7 for $D_{combustor}$=10cm and in fig. 8 for ER=1.0. Results show that temperatures rate of decrease is higher on the edge the burner.

Figure 7. should be placed here

Figure 8. should be placed here

Tab. 5 reports the maximum temperature achieved by the burned gases as a function of the ethylene temperature at burner entrance (ER=1.0). The low value of fuel to oxidizer mass flow ratio (about 1/15) renders the effect of fuel heating on combustor temperatures quite small. As a practical consequence for the mock-up, the nozzle device expected to decrease the fuel pressure to ensure atmospheric combustion does not require to be heated. Its cooling effect on the fuel flow (due to its high thermal inertia) will not significantly affect flame temperature inside the combustor.

Table 5. should be placed here

Fig. 9 shows the results of numerical analysis for ER=1.0, in dependence of $D_{combustor}$ values, on the temperatures achieved by the fuel flowing into the rolled-up tube. All the other parameters (fuel jet features, materials properties, boundary conditions) are kept as constant, the values being those defined above.

Figure 9. should be placed here

For a given value of ER, diameter decrease determines a general raise in the ethylene temperatures. That does not represent a surprise, as the further the diameter increase, the further the density of both convective and radiative heat flux from the burned gases to the rolled-up channel eases off. It is worth noting that ethylene temperatures found at the exit of the cooling channel inevitably overestimate those the fuel would achieve in real operation, as the numerical analysis does not take into account the enhancement of fuel cooling capacity due to pyrolysis endothermic behavior (only its sensible heat sink was considered). To better highlight the effect of equivalence ratio, fig. 10 is reported. For $D_{combustor}$=10 cm value, temperature profiles of ethylene are represented, along the cooling channel, as a function of ER.

Figure 10. should be placed here

ER impacts directly the burned gases temperatures, whose maximum is in stoichiometric conditions (ER=1.0). So, independently of the diameter, decreasing ER from 1.0 to 0.8 causes a general lowering of heat transfer density and consequently of the temperatures of the ethylene flowing into the tube.

The comparison of data reported in fig. 9 and 10 shows that the effect on ethylene heating of the diameter $D_{combustor}$ is huger than that of equivalence ratio ER. That is probably because the importance of equivalence ratio variations is higher when a strong radiative heat transfer is present (it depends on the fourth power of burned gases temperatures, which vary with ER). That is not the case, as no reach combustion is considered. So the effect of a decrease in the gases temperatures due to the passage to a lean combustion counts for less than that due to the raise in the area of the surface exposed to them, which vary with the second power of $D_{combustor}$.

Fig. 11 illustrates the variations of total (convective + radiative) heat flux density from the hot gases to the cooling channel at different values of $D_{combustor}$ in dependence of ER.

Figure 11. should be placed here

This parameter strongly depends on $D_{combustor}$, while its variations with equivalence ratio are less relevant, even if they are present. Overall, heat flux density ranges from a minimum of 7420 w/m^2 ($D_{combustor}$=12cm, ER=0.8) to a maximum of 10295 w/m^2 ($D_{combustor}$=8cm, ER=1.0). It could be expected in case of pyrolysis that the endothermic pyrolysis reactions act as an heat sink. As a result, the total heat flux exchanged by flue gas with hot wall would increase and be higher than the above estimated values.

Fig. 12 illustrates the variations of the maximum temperature achieved by the rolled-up tube wall for the three values of $D_{combustor}$ examined, as a function of ER.

Figure 12. should be placed here

Being a strong function of heat flux density, the trends shown in fig. 12 resemble those reported in fig. 11. Maximum temperature vary both with the diameter of the combustion chamber and with equivalence ratio. As already mentioned at the beginning of section 3.1, the numerical simulated results may overestimate the real operating data. This point is, in this context, very relevant, because of the necessity to act in order not to get temperatures which the constituting material can not withstand. Thus, the safety coefficient that should be applied will not be required since overestimation from simulation will be considered as serving for safety margin.

The evaluation of the residence time of the fuel into the cooling channel is a challenging point. According to the results of numerical simulations the fuel flowing into the cooling channel can be heated at temperatures which are consistent with those required to get its decomposition (about 1200 K) very quickly. So, being the composition of the fluid flowing into the channel unknown for most of its run, it is quite difficult to get precise information on its density. Moreover, no reliable models are nowadays at our disposal to correlate supercritical fluids properties to pressure and temperature. On the basis of the data found on the website of N.I.S.T. [22], for a pressure of 50 bar and a temperature of 1200 K, a density for ethylene ranging between 70 and 100 kg m^{-3} should be expected. Using it as a reference, considering the internal diameter of the cooling channel and the propellant mass flow rate, velocities between 0.27 and 0.38 m s^{-1} could be achieved.

Assuming the density of ethylene to be constant along the cooling channel, an estimation of the residence time is possible. Results are reported in tab. 6. They clearly show that residence time is always higher than 100 s; which is enough to get pyrolysis within the cooling channel, even with moderate fuel temperature. At the authors knowledge, there are no studies on ethylene pyrolysis in such a configuration. Studies carried out on similar

configurations on different fuels reported, for example, that a conversion rate of 100% is obtained for n-dodecane at 1400 K, with a residence time of 7.6 s [5]. Considering that a residence time of at least one order of magnitude higher is expected, the complete decomposition of the fuel should be easily obtained.

Table 6. should be placed here

3.2. Dynamics characterization and similitude rules

As already said in paragraph 2.1, 0-D analytical calculations have been performed. A reaction enthalpy of 42 MJ/kg has been considered for n-dodecane combustion, while a reaction enthalpy of 1.43 MJ/kg has been considered for n-dodecane pyrolysis decomposition [24]. A combustion chamber height $H_{combustor}$ of 20 cm, a thickness of the wall separating the burned gases and the fuel of 2 mm, a cooling channel thickness of 2 mm, a pressure of 3 MPa were chosen. Stoichiometric combustion is considered.

The results are shown in tab. 7:

Table 7. should be placed here

It is observed that the rise of fuel mass flow rate favors fuel pyrolysis as it strongly impacts the combustion heat flux, thus the heat flux density received by the fuel flowing through the cooling channel. Despite heat loss increases from 23% to 37% when increasing it from 0.07 to 0,285 g s^{-1}, the overall fuel mass flow rate effect consists in an improvement of heat transfer.

A temperature of 835 K is obtained in case of a mass flow rate of 0.107 g/s; which seems to be, when n-dodecane is used, a good compromise to get pyrolysis (considering the residence time) similar to the one on realistic engine (conversion rate over 50%) [5,19].

Similitude rules have been taken into account in designing the experimental test bench. The values of the main parameters are comparable with a real scramjet engine, as shown in tab. 8:

Table 8. should be placed here

3.3. Discussion of the results

Fluent analysis showed that goals 1 and 2 (paragraph 3) can be achieved both by using 10 cm diameter and 8 cm diameter combustion chambers. Fuel temperatures observed at the outlet of the rolled-up tube when $D_{combustor}$=12 cm would be just on the limit. Considering the above mentioned general fuel temperatures overstating, a 12 cm diameter combustor is considered inadequate. The choice reduced to 8 cm and 10 cm diameter combustion chambers, it has been decided to opt for the second possibility. When compared to the 8 cm tube, in fact, the 10 cm one presents two important advantages:

1. the maximum temperature of the cooling channel wall fall just under the upper limit;
2. the residence time of the propellant into the tube is higher (of about 20%), and consequently the duration of its exposure to the flame heat load is greater.

The second point is crucial. Clearly, variations in the combustion chamber diameter are accompanied by variations in the length of the rolled-up tube. That determines a change in the permanence of the fuel in the combustion chamber: consequently the greater is the combustor diameter, the highest is the duration of its exposure to the flame heat load. That enhances fuel decomposition.

Moreover, by varying the ratio between the fuel and the oxidizer mass flow rates it is possible to act on both the temperatures achieved by the ethylene flowing through the cooling channel and by its wall. That will allow to change the enhancement of pyrolysis phenomena and, if necessary, to avoid the material to be exposed to too high temperatures.

Thanks to this pre-dimensioning work, the optimum test bench was designed. It is constituted by a pilot burner allocated into a small cylindrical combustion chamber. Before being injected into the burner, the fuel (previously brought at supercritical pressure) is forced to flow through a rolled-up stainless steel tube, having the form of an helix, passing into the combustion chamber. The flame is positioned right at the center of the combustor. The process is operated at ambient pressure and so the propellant, that is in supercritical condition at the exit of the helix-like tube, must be depressurized by using a nozzle-like device.

The use of National Instruments PXI remote controllers ensure remote control of the experimental test bench. All the devices can be automatically commanded from a computer by means of NI Labview system design and control software.

The schemes of the experimental test bench and of the combustion chamber are represented in fig. 13.

Figure 13. should be placed here

Apart from pressure reducers P1 and P2, all the devices represented are remotely commanded by Labview. They are listed as follows.:

- Pressure Reducers PC1, PC2;
- Electrovalves V1, V2, VC1, VC2;
- Pressure Transmitter PT;
- Mass Flow Controllers MFM1, MFM2;
- Burner B.

4. Conclusions

The need for a remote-controlled experimental bench reproducing a ramjet combustion chamber has been expressed for latter developing regulation and control strategies

(regeneratively fuel-cooled engine). A specific study with appropriate similitude rules is required. This work falls within the high speed flight framework and faces the related challenge of structures cooling. The dual and coupled functions of the fuel (coolant/propellant) impose to define well the test bench in terms of dynamics, heat flux density, pyrolysis rate and chemical composition. The present work focuses on the dimensioning of such a high-end system whose complexity in terms of scientific and engineering concepts required simultaneously CFD calculations and analytical approaches. As a result, it was shown that a range of equivalence ratio ranging from 0.8 to 1.0 can be obtained with fuel flow rate from 70 to 100 mg/s and pressure up to 50 bar. That corresponds to a residence time of the fuel within the cooling channel of about 100-200 s, a maximum temperature of pyrolysed fuel of 1200-1300 K, and a heat flux density of 7000-10000 W m^{-2}. The final bench features have been defined (combustor diameter of 10 cm, a cooling channel length of 47.5 m). A similitude rule has been obtained after choosing carefully all the operating and geometrical parameters. Particularly, the ratio of heat flux density over fuel mass flow rate for the experiment (about 0.1-1.0 MJ kg^{-1} m^{-2}) is similar to the realistic one expected for a full scale engine. It has been shown that the cooling effect on burned gases temperature of the nozzle-like device is quite negligible. Realistically, complete conversion of fuel by pyrolysis can be easily obtained, thanks to the high value of the residence time into the cooling channel, even if its final temperature is under 1300 K (the value expected on the basis of CFD simulation). Analytical calculations carried out on a similar configurations have demonstrated that an increase in fuel mass flow rate determine an increase in the temperature of the fuel exiting from the cooling channel (because of dominant effect on the combustion heat flux). The on-going step is now to conduct the experiments to qualify and characterize the dynamics of phenomena for latter proposing a simplified model to which a regulation

strategy could be applied. The results of the experiments will allow validating those that can be obtained by means of numerical simulations.

Figures

Figure 1. Fuel mass flow rate increase: negative loop in terms of thrust variation

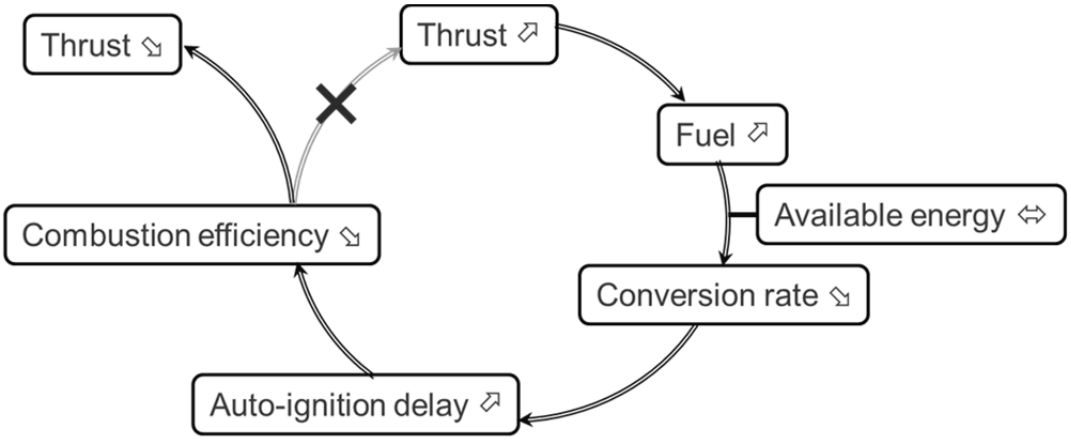

Figure 2. Scheme of the system considered to perform analytical calculations

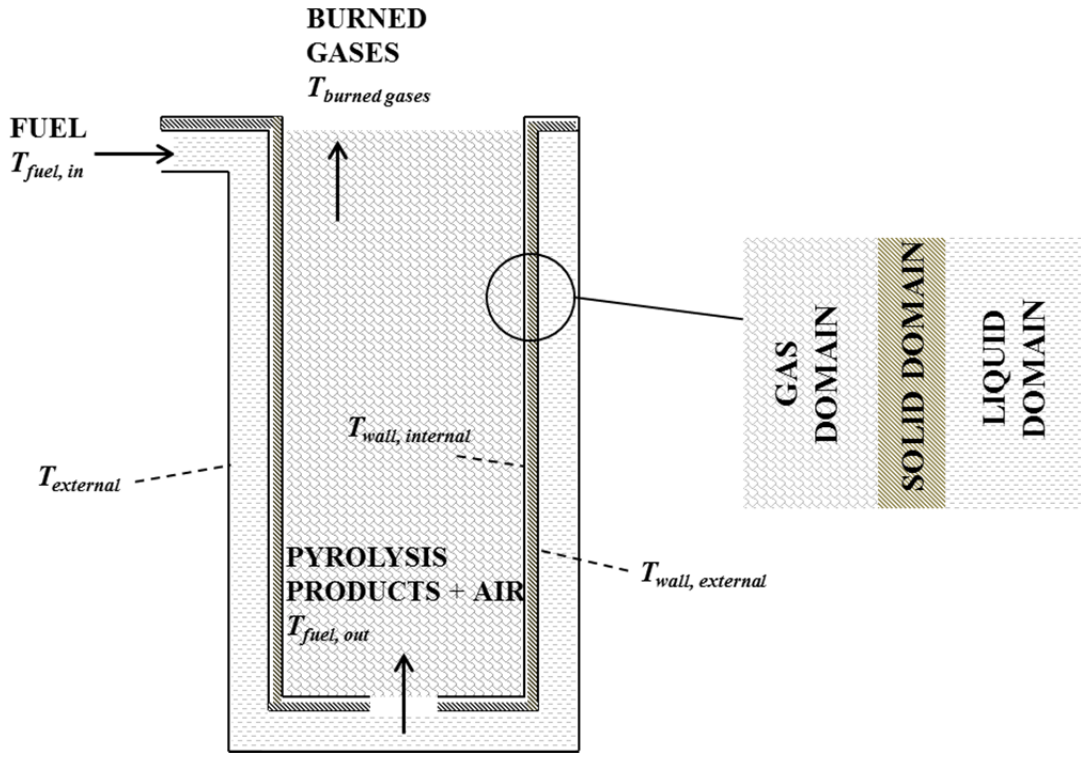

Figure 3. Schematic of the nozzle that will be inserted along the line carrying the fuel to the burner

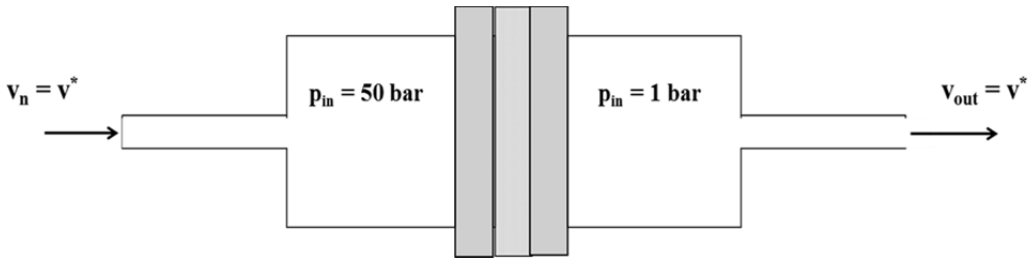

Figure 4. Schematic of the configuration adopted to reproduce the combustor

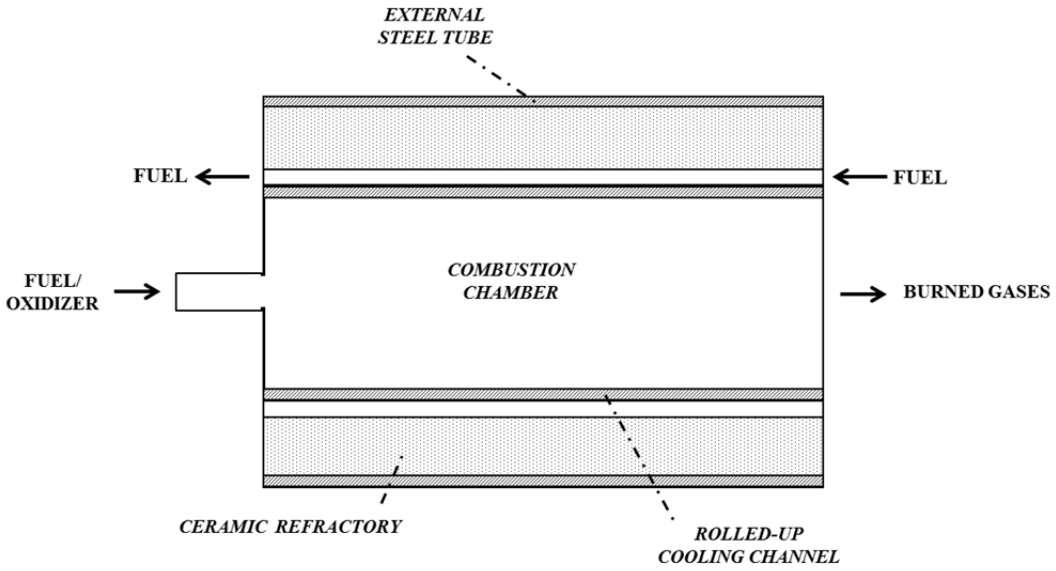

Figure 5. Case $D_{combustor}$=8cm, general view of the grid (a) and of its initial part (b)

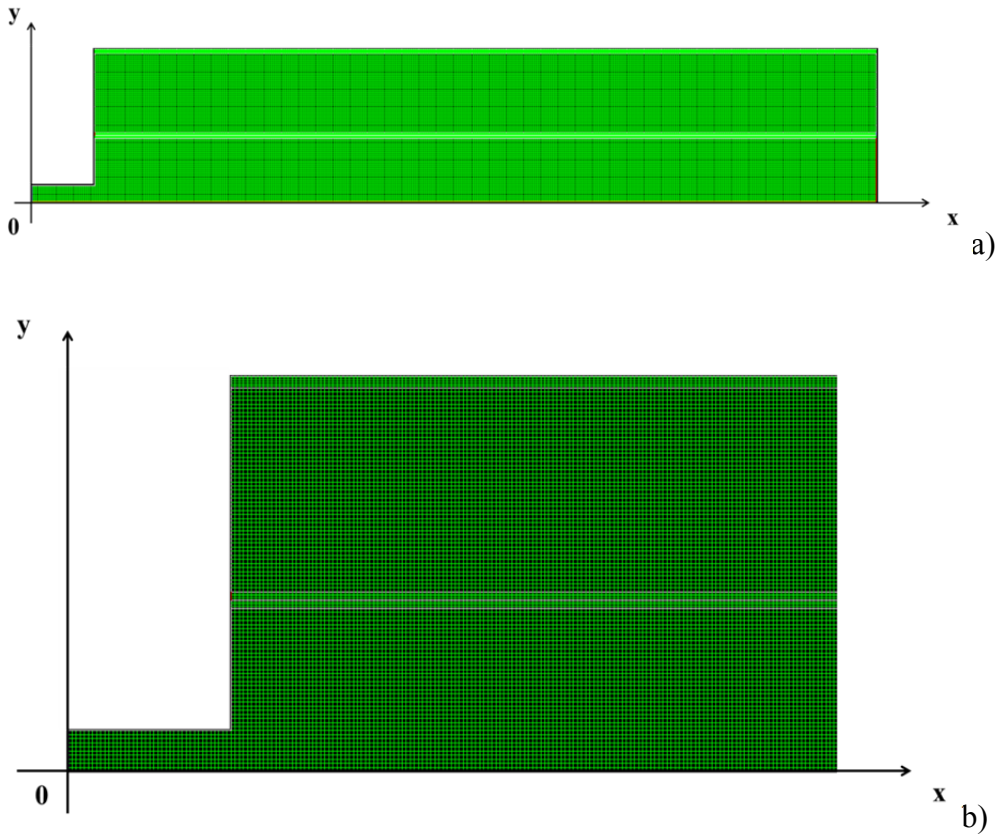

Figure 6. Schematic representing the imposed boundary conditions

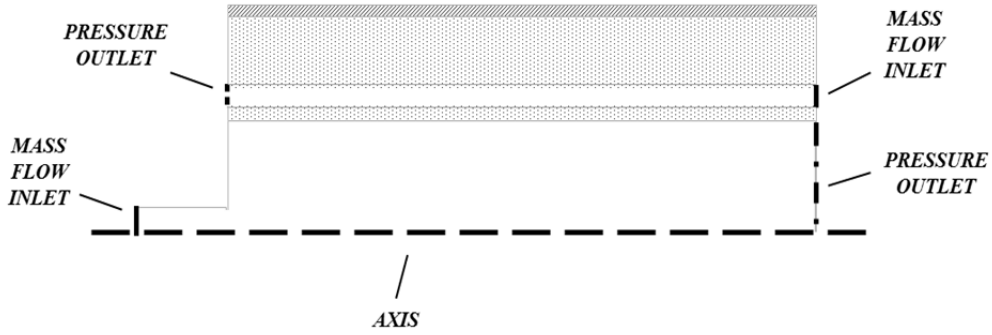

Figure 7. Temperature contours in the computed domain for a combustor diameter of 10 cm and an Equivalence Ratio of 1.0 (a), 0.9 (b) and 0.8 (c)

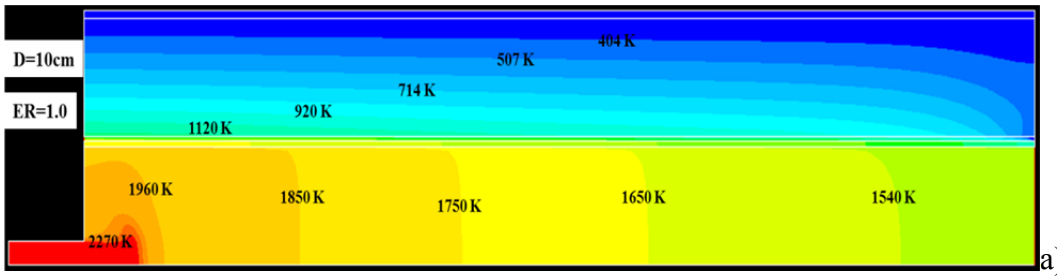

a)

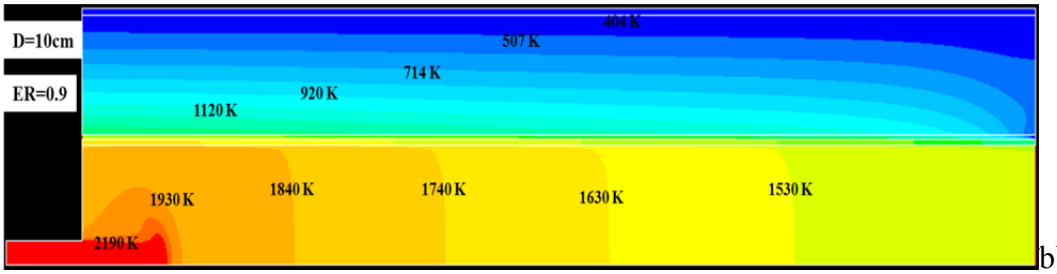

b)

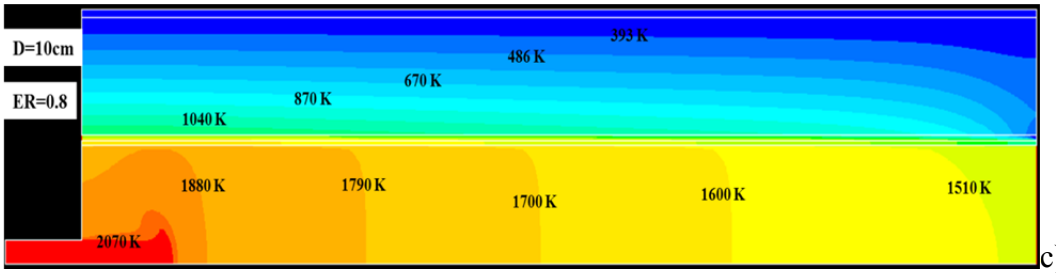

c)

Figure 8. Temperature contours in the computed domain for an Equivalence Ratio of 1.0 and a combustor diameter of 8 cm (a), 10 cm (b) and 12 cm (c)

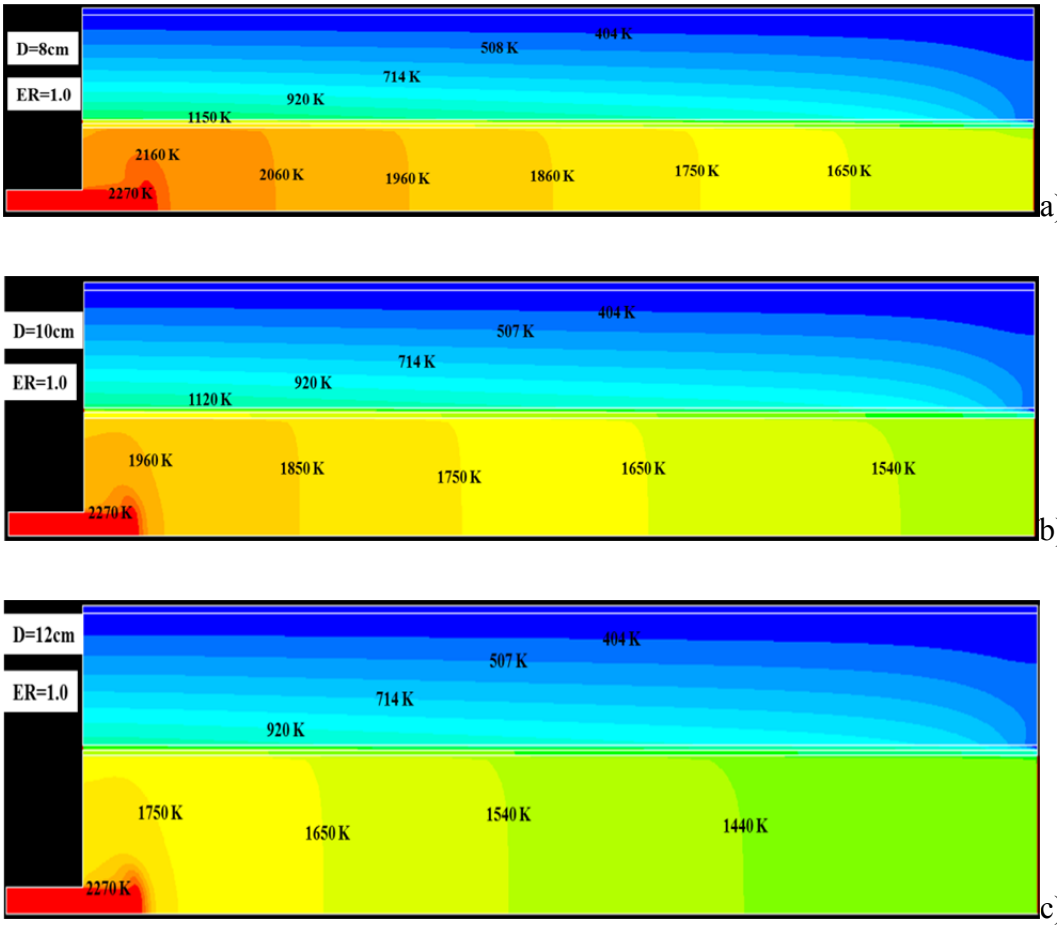

Figure 9. Fuel temperature profiles along the cooling channel for ER=1.0 (as a function of combustor diameter).

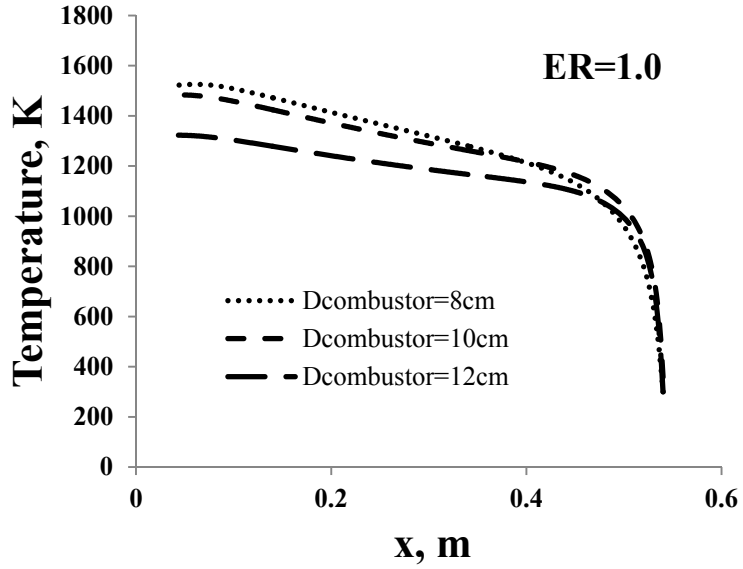

Figure 10. Fuel temperature profiles along the cooling channel, for $D_{combustor}$=10cm (as a function of equivalence ratio).

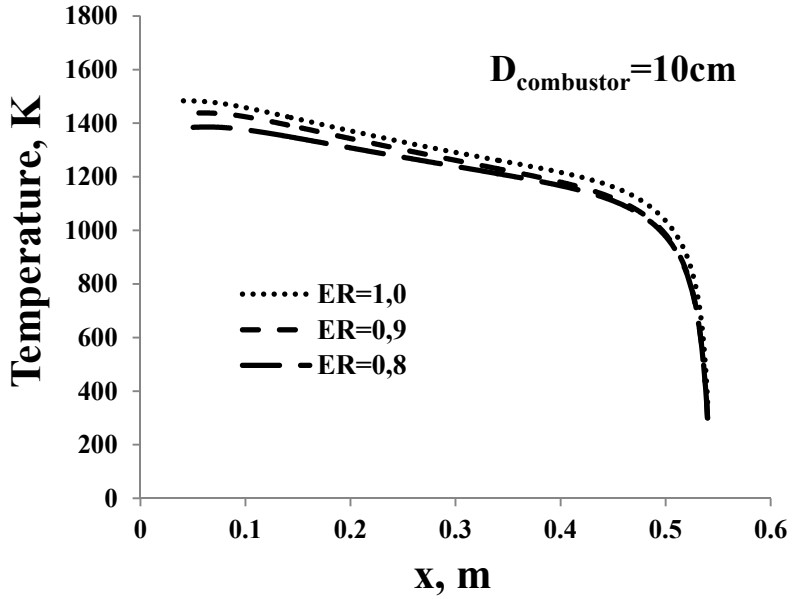

Figure 11. Total heat flux density from flue gas to hot wall as a function of ER at different values of $D_{combustor}$

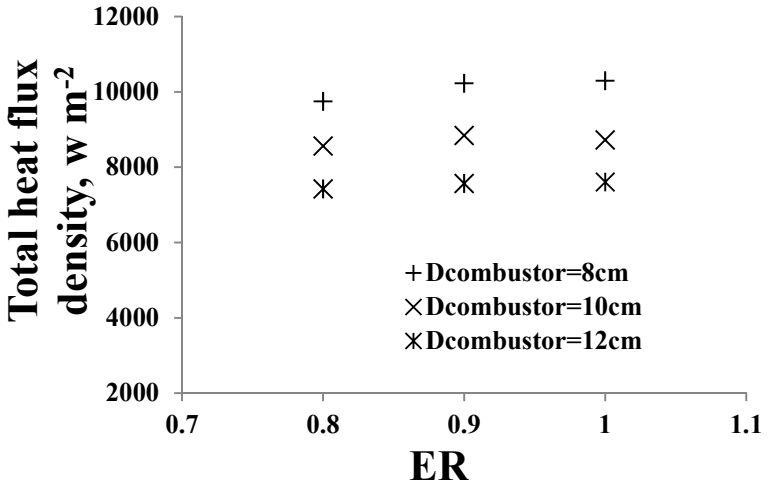

Figure 12. Variations of cooling channel wall maximum temperature at different values of D considered, in dependence of ER

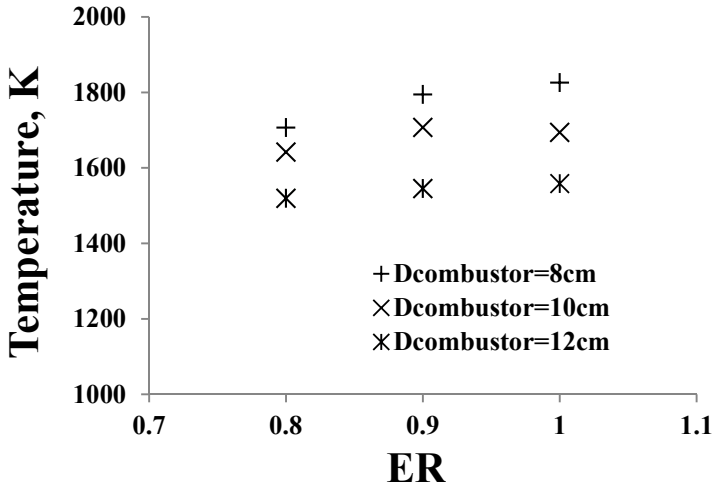

Figure 13. Experimental test bench scheme (a) and combustion chamber (b)

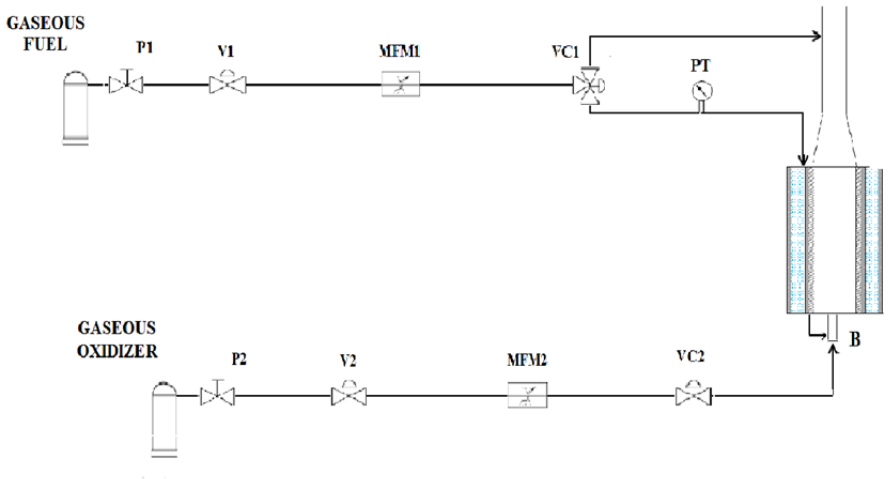

a)

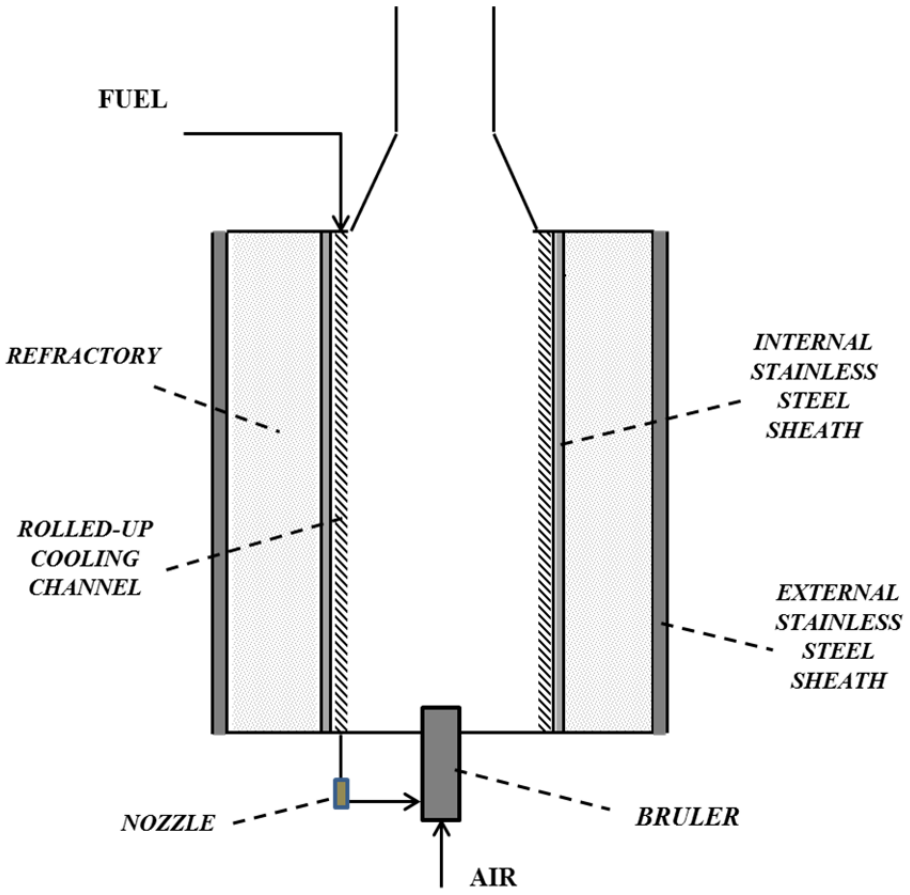

b)

Tables

Table 1. Grids main features

D (cm)	Cells	length (mm)	height (mm)	y^+
8	52400	540	97	>5 / < 40
10	57400	540	107	>5 / < 40
12	62400	540	117	>5 / < 40

Table 2. Characteristics of the jet injected into the computational domain

ER	1	0,9	0,8
$\dot{m}_{fuel}$(g s^{-1})	0,1	0,1	0,1
$\dot{m}_{oxid}$(g s^{-1})	1,47023	1,63359	1,83779

Table 3. Defined physical properties of stainless steel tubes and ceramic refractories blanket

	ρ (kg m^{-3})	c_p (J kg^{-1} K^{-1})	k_{ther} (w m^{-1} K^{-1})
Stainless Steel	8030	502,48	16,27
Refractory	128	1030	0,33

Table 4. Reynolds number in the combustion chamber. Cross-section average values are considered for viscosity μ, density ρ and velocity v.

μ/ρ (m^2 s^{-1})	v (m s^{-1})	$D_{combustor}$ (m)	$Re_{combustor}$
10^{-5}-10^{-4}	10^{0}-10^{1}	10^{-1}	10^{3}-10^{5}

Table 5. Trend of adiabatic flame temperature of burned gases in function of the temperature of ethylene injected in the burner

$T_{ethylene}$ (K)	$T_{ethylene+air}$ (K)	$T_{adiabatic}$ (K)
300	300,0	2370,4
400	311,0	2374,9
500	325,1	2380,6
600	341,1	2387,1
700	358,5	2394,4
800	376,8	2401,6
900	395,6	2408,9
1000	414,7	2416,9

Table 6. Estimation of fuel residence time in the cooling channel, respectively for v=0.27ms^{-1} and v=0.38ms^{-1}

$D_{combustor}$ (m)	$L_{combustor}$ (m)	$t_{r,min}$ (s)	$t_{r,max}$ (s)
0,08	39,56	146,9	102,8
0,10	49,45	183,6	128,5
0,12	59,34	220,4	154,2

Table 7. Evolution of fuel temperature at combustor injection, heat losses and heat flux density from combustor to cooling channel as a function of fuel mass flow rate

	Fuel Mass flow rate (g s^{-1})	Maximum fuel temperature at combustor injection (K)	Heat loss due to burned gases evacuation from the combustor (% of total produced heat)	Heat Flux Density from Combustor to cooling channel (W/m^2)
Case 1	0,07	700	23%	2655
Case 2	0.107	835	29%	4483
Case 3	0,285	1200	37%	11955

Table 8. Comparison between the values of the main parameters characterizing a real scramjet engine and those expected from the designed experimental facility

Parameters	Real Scramjet Engine	Representative Experiment
Residence time in the cooling channel (s)	5 – 10 [5]	100 - 200
Combustion heat flux density from combustion chamber (W kg^{-1} m^{-2})	$2 – 40 \cdot 10^7$ [5,8]	$7 – 10 \cdot 10^7$
Pyrolysis rate (%)	50-100 [5,15]	100
Fuel enthalpy of decomposition (J kg^{-1})	$1.43 \cdot 10^6$	$1 - 1.5 \cdot 10^6$

Maximum coolant temperature (K)	1500 [25]	1200 - 1300
Maximum wall temperature (K)	1600 [5]	1400-1500

References

[1] U.M. Schoettle, H. Grallert, F.A. Hewitt, *Advanced air-breathing propulsion concepts for winged launch vehicles*; Acta Astronautica, Volume 20, Pages 117-129 (1989)

[2] Y.M. Timnat, *Recent developments inramjets, ducted rockets and scramjets*; Progress in Aerospace Sciences, Volume 27, Issue 3, Pages 201-235 (1990)

[3] R.S. Fry, *A Century of Ramjet Propulsion Technology Evolution*; Journal of Propulsion and Power, Volume 20, No. 1, January-February 2004

[4] E.T. Curran, *Scramjet engine: the first forty years*; Journal of Propulsion and Power, Volume 17, No. 6, Pages 1138-1148 (2006)

[5] N. Gascoin, P. Gillard, *Dynamic study of coupled heavy hydrocarbon pyrolysis and combustion*; Combustion Science Technology (2012)

[6] W. Bao, J. Qin, W. X. Zhou, D. R. Yu, *Effect of cooling channel geometry on re-cooled cycle performance for hydrogen fueled scramjet,* International Journal of Hydrogen Energy, No. 35, Pages 10589-10598 (2010)

[7] A. Ulas, E. Boysan, *Numerical analysis of regenerative cooling in liquid propellant rocket engines*; Aerospace Science and Technology, Volume 24, Pages 187-197 (2013)

[8] J. Qin, W. Bao, W. X. Zhou, D. R. Yu, *Flow and heat transfer characteristics in fuel cooling channels of a re-cooling cycle*, International Journal of Hydrogen Energy, Number 35, Pages 7002-7011 (2010)

[9] W. Yang, B. Sun, *Numerical simulation of liquid film and regenerative cooling in a liquid rocket*; Applied Thermal Engineering, Volume 54, Issue 2, Pages 460-469 (2013)

[10] D. R. Bhata, M. D. Carey, J. G. Campell, C. D. Coulbert, *Thrust Chamber Cooling Techniques for Spacecraft Engines*; The Marquardt Corporation, Volume 2, Project 278 (1963)

[11] L. Schoerman, *High-pressure propulsion-advanced concepts for cooling*; Acta Astronautica, Volume 14, Pages 423–438 (1986)

[12] S.K Kima, J. Miok, S. C. Hwan, S. P. Tae, *Multidisciplinary simulation of a regeneratively cooled thrust chamber of liquid rocket engine: Turbulent combustion and nozzle flow*; International Journal of Heat and Mass Transfer, Volume 70, Pages 1066–1077 (2014)

[13] G. Yu, J.G. Li, , X.Y. Chang, L.H. Chen, C.J. Sung, *Investigation of kerosene combustion characteristics with pilot hydrogen in model supersonic combustors*; Journal of Propulsion and Power, Volume 17, No. 6, Pages 1263–1272 (2001)

[14] L. Y. Hou, N. Dong, D. P. Sun, *Heat transfer and thermal cracking behavior of hydrocarbon fuel*; Fuel, Volume 103, Pages 1132-1137 (2013)

[15] N. Gascoin, P. Gillard, S. Bernard, M. Bouchezb, *Characterization of coking activity during supercritical hydrocarbon pyrolysis*; Fuel processing technology, Volume 88, Number 12, Pages 1416-1428 (2008)

[16] G. Fau, N. Gascoin, P. Gillard, M. Bouchez, J. Steelant, *Fuel pyrolysis through porous media: coke formation and coupled effect on permeability*; Journal of Analytical and Applied Pyrolysis, Number. 95, Pages 180-188 (2012)

[17] G. Z. Liu, X. Q. Wang, X. W. Zhang, *Pyrolytic depositions of hydrocarbon aviation fuels in regenerative cooling channels*; Journal of Analytical and Applied Pyrolysis, Volume 104, Pages 384-395 (2013)

[18] FLUENT® Inc. 6.3.23 User's Guide, Chapter 12 (2006)

[19] M. H Back, *Pyroysis of Hydrocarbons*; The mechanisms of pyrolysis, oxidation, and burning of organic materials (National Bureau of Standards Special Publication 357), Pages 17-25 (1972)

[20] R.G. Compton, C.H. Iamford, C.F.H. Tipper, *Decomposition and Isomerization of Organic Compounds*; Chapter 4, Pages 59-62 (1972)

[21] X. Q. Wang, Z. Tao, T. Y. Song, L. H. Han, *Stress–strain model of austenitic stainless steel after exposure to elevated temperatures*; Journal of Constructional Steel Research, Volume 99, Pages 129-139 (2014)

[22] http://webbook.nist.gov/chemistry/

[23] K.D. Dahma, P.S. Virkb, R. Bounaceurc, F. Battin-Leclercd, P.M. Marquaired, R. Fournetd, E. Daniaue, M. Boucheze, *Experimental and modelling investigation of the thermal decomposition of n-dodecane*; Journal of Analytical and Applied Pyrolysis, Volume 71, Issue 2, Pages 865-881 (2004)

[24] N. Gascoin, P. Gillarda, M. Bouchezb, *Chemical composition and mass flow measurements in a supercritical reactive flow for hypersonic real-time application*; Aerospace Science and Technology, Volume 14, Issue 4, Pages 266-275 (2010)